

Optimal Nonlinear Line-of-Flight Estimation in Positron Emission Tomography

Alexander M. BRONSTEIN, Michael M. BRONSTEIN, Michael ZIBULEVSKY and Yehoshua Y. ZEEVI

Abstract-- We consider detection of high-energy photons in PET using thick scintillation crystals. Parallax effect and multiple Compton interactions such crystals significantly reduce the accuracy of conventional detection methods. In order to estimate the photon line of flight based on photomultiplier responses, we use asymptotically optimal nonlinear techniques, implemented by feed-forward and radial basis function (RBF) neural networks. Incorporation of information about angles of incidence of photons, significantly improves accuracy of estimation. The proposed estimators are fast enough to perform detection, using conventional computers. Monte-Carlo simulation results show that our approach significantly outperforms the conventional Anger algorithm.

Index Terms—emission tomography, gamma camera, scintillation detector, artificial neural network.

I. INTRODUCTION

DETECTION of high-energy photons emitted as the result of positron decay is one of the most important low-level stages in PET imaging. In this paper we consider a detector based on the Anger scintillation camera [1]. Incident high-energy gamma quanta, generated due to positron decay, produce scintillation effect in the crystal. As the result, a shower of low energy photons in the visible and UV spectra is emitted. These photons are collected by an array of photomultipliers (PMTs), optically coupled to the scintillation crystal, and invoke electric impulses in them. The PMT responses are utilized in estimation of the scintillation point coordinates.

A non-collimated Anger camera, based on thick crystals with high photon penetration depth such as NaI(Tl), is considered in this work. Application of such thick crystals in PET scanners is desirable, due to their low cost and very high light output; they were previously used primarily in gamma ray astronomy [2].

The majority of existing scintillation position estimation

algorithms are based on centroid arithmetic, usually combined with correction maps [3]. Their application appears, however to be problematic in the case of thick crystals due to significant parallax observed at large radiation incidence angles.

Tomitani et al [4] proposed an iterative maximum likelihood algorithm for position estimation and depth encoding in thick scintillation crystals, in order to compensate for the parallax effect. However, an iterative approach necessitate extensive computations that prohibit real-time implementation.

Delorme et al [5] and Clément et al [6] have implemented artificial neural networks in a depth-encoding scintillation detection. The approach is flexible and offers advantages over iterative algorithms. Still, it does not resolve the problem of multiple Compton interactions, which make the conception of "depth of interaction" ambiguous.

Our work presents a solution for these problems, incorporating side information on the photon incidence angle into the process of position estimation. We use localized, asymptotically optimal, nonlinear estimators, implemented by feed-forward and radial basis functions (RBF) neural networks. As a byproduct, we get accurate position estimation over the entire area of detector including the edges. This is difficult to obtain with centroid arithmetics algorithms. We present a comparison of algorithms on a Monte Carlo simulation and discuss the prospects for practical implementation.

II. ESTIMATION OF SCINTILLATION COORDINATES

In order to estimate the line of flight, it is usual to estimate coordinates of interaction independently in each detector. The situation becomes more complicated in presence of Compton interactions. Even in the simple case of a single Compton interaction, with consequent photoelectric absorption, one can attempt to estimate the coordinates of both interactions, and choose one with lower penetration depth. A more accurate decision would be to choose the first interaction along the possible line of flight. This observation demonstrates the importance of prior knowledge of photon direction.

Due to limited light statistics, the coordinate estimate is not perfect, and one can use the Bayesian framework to optimize it. This would involve knowledge of the distribution of energy deposit and consequent flight directions at every Compton interaction, probability of photoelectric absorption, distribution of visible photons after each interaction etc. Finally we would obtain a complicated estimator, which gives

Manuscript received March 8, 2002. This research has been supported in part by the Ollendorff Minerva Center, by the Fund for Promotion of Research at the Technion, and by the Israeli Ministry of Science.

A. M. Bronstein (e-mail: bron@aluf.technion.ac.il), M. M. Bronstein (e-mail: bron@tx.technion.ac.il), M. Zibulevsky (e-mail: mzib@ee.technion.ac.il) and Y. Y. Zeevi (e-mail: zeevi@ee.technion.ac.il) are with the Technion – Israel Institute of Technology, Department of Electrical Engineering, Haifa 32000, Israel.

a coordinate of the first interaction. The resulting model should include initial photon direction. The problem does not seem to be easily solvable, especially in real time.

As an alternative, we use a learning approach in order to build and solve the approximation of the optimal statistical model automatically, using training data, which can be available in large amounts from simulation or from physical experiment. Relatively computationally intensive training process results in fast and accurate on-line estimator.

Our crucial observation is that using the knowledge of photon direction, one can get a more accurate estimate. In this case one do not even need to estimate the 3D coordinates of each interaction. Instead, the 2D coordinate of photon entrance into the detector crystal can be estimated directly. Together with the incidence angle, this gives full description of the line of flight.

Such an approach reduces the influence of the parallax effect and multiple Compton interactions, since the point of photon entrance is well-defined in this case as well (Figure 1). Unlike many existing approaches, our method does not rely on the average interaction depth.

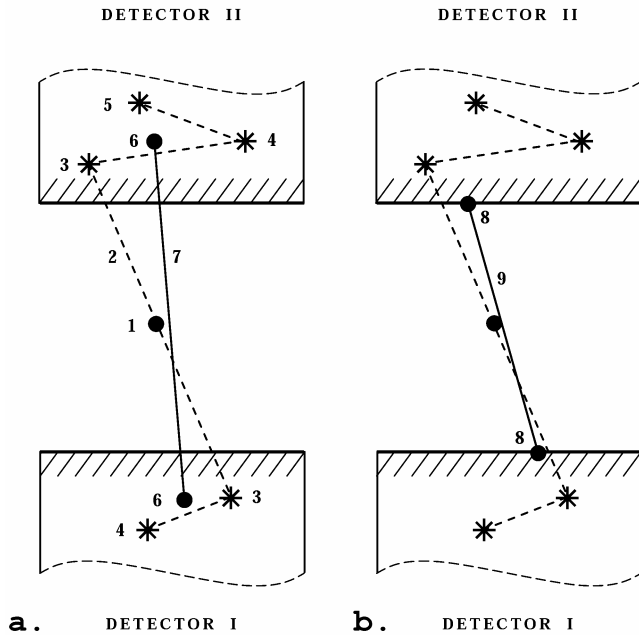


Fig. 1. Scheme of photon coordinate estimation using the Anger algorithm (a) and ANN-based estimator (b). 1 – photon pair emission source, 2 – actual line of flight, 3 – first interaction, 4 – secondary interaction, 5 – tertiary interaction, 6 – scintillation point estimated by Anger algorithm, 7 – LOF estimated by Anger algorithm, 8 – entrance point estimated by ANN, 9 – LOF estimated by ANN.

III. PARAMETRIC ESTIMATION USING NEURAL NETWORKS

Scintillation detector can be considered to be a complicated non-linear stochastic system that maps the photon line of flight (LOF) into a vector \mathbf{x} of PMT responses. Given the incidence angle, LOF is defined by planar coordinates $\mathbf{y} = (y_1, y_2)$ on the surface of the crystal. For every incidence angle, we implement an optimal nonlinear estimator of \mathbf{y} of the form

$\hat{\mathbf{y}} = \Phi(\mathbf{x}; \mathbf{W})$, where $\Phi(\mathbf{x}; \mathbf{W})$ is a family of functions, parameterized by the vector of parameters \mathbf{W} .

A reasonable criterion for estimator optimality is the expectation of some error function $\mathbb{E}\{\mathcal{E}(\Phi(\mathbf{x}; \mathbf{W}) - \mathbf{y})\}$, for example, the expected squared error $\mathbb{E}\{\|\Phi(\mathbf{x}; \mathbf{W}) - \mathbf{y}\|_2^2\}$.

We are interested in forms of $\Phi(\mathbf{x}; \mathbf{W})$, that possess the property of a universal approximator: when the number of parameters \mathbf{W} is large enough, any bounded function $f(\mathbf{x})$ can be approximated with given accuracy over a bounded domain by an appropriate choice of \mathbf{W} .

Given the PMT responses to a set of known LOFs $\{\mathbf{y}^i; \mathbf{x}^i = f(\mathbf{y}^i) = (x_1^i, \dots, x_n^i)\}_{i=1}^N$ (referred to as a *training set*), we find such \mathbf{W} , that minimizes the mean-squared error (MSE) on the training set, i.e:

$$\mathbf{W}^* = \underset{\mathbf{W}}{\operatorname{argmin}} \sum_{i=1}^N (\Phi(\mathbf{x}^i; \mathbf{W}) - \mathbf{y}^i)^2.$$

This process is referred to as *training*. When the training set is sufficiently large, the MSE approximates the expected squared error with any desired accuracy. Under such conditions, a universal approximator $\Phi(\mathbf{x}; \mathbf{W}^*)$ with sufficient parameters approaches the optimal non-linear estimation.

In this work we used two types of universal approximators implemented as artificial neural networks (see Appendix for description).

IV. TWO-LEVEL SCHEME USING LOCALIZED ESTIMATORS

Our scheme is based on a combination of coarse and fine estimators (Figure 2). Fine estimators, implemented as artificial neural networks, are trained on scintillation events in different (possibly overlapping) regions at a range of calibrated incidence angles. Coarse estimators, based, for example, on the Anger algorithm determine the rough position and incidence angle of the photon. According to this information, the appropriate fine estimator is selected. Such a combination of estimators allows reduction in the size of each network and accelerates the training.

V. SIMULATIONS

In order to test the proposed approach and compare it with other algorithms, we performed a Monte Carlo simulation of ray tracing and gamma quanta interaction in a scintillation detector. The simulation was performed using a slightly modified version of TRIUMF detector modeling platform introduced by Tsang et al [8], [9]. The region of interest and the incidence angle involved in the estimator selection were assumed to be known.

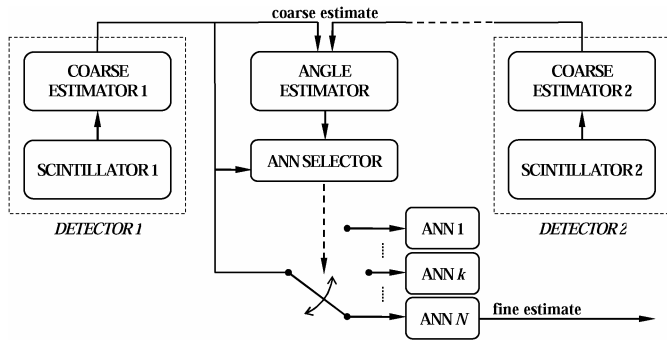


Fig. 2. Block diagram of a practical ANN-based scintillation coordinates estimation algorithm: estimation of scintillation coordinates in detector 1 using side information from detector 2.

A model of a NaI(Tl) scintillation crystal of size $210 \times 210 \times 45$ mm, separated with a 20 mm glass light guide was simulated. The detector consisted of seven circular PMTs, each of radius 30 mm, with inter-tube gaps of 10 mm. The inter-tube area was assumed to consist of an ideal light-absorbing material (Figure 3). Figure 4 depicts the coordinate system of the detector model.

Using TRIUMF, we simulated narrow beams of 512 KeV gamma quanta impinging at the detector crystal surface in a given point at a given incidence angle. The point at which the beam entered the scintillator surface was recorded for each simulated event and served as reference for position estimation. Incidence angle was measured as shown in Figure 5.

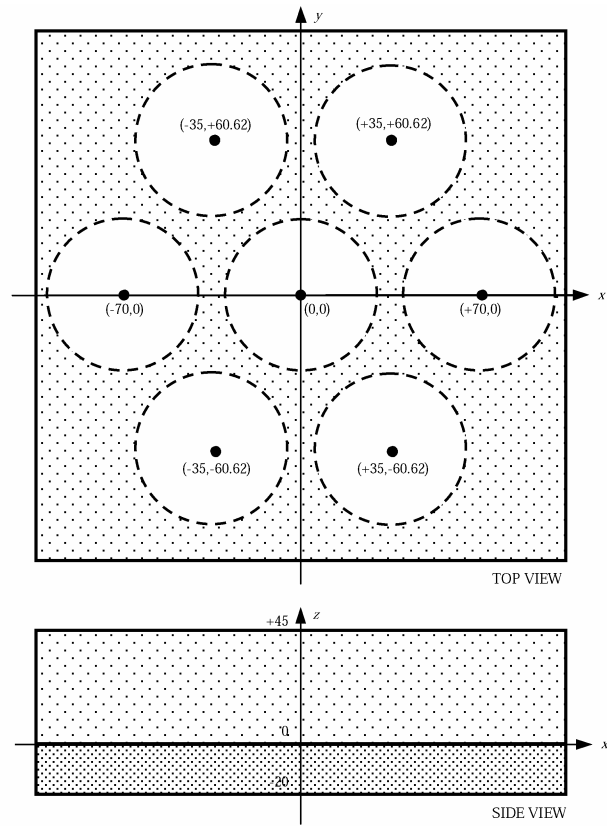


Fig. 4. Detector coordinate system. All coordinates are given in mm.

PMT responses to the simulated scintillation events, expressed as the number of the produced photoelectrons (assuming quantum efficiency of 25%) were recorded. Pulse spectrum (Figure 6) was estimated in order to determine the threshold for low-energy events rejection.

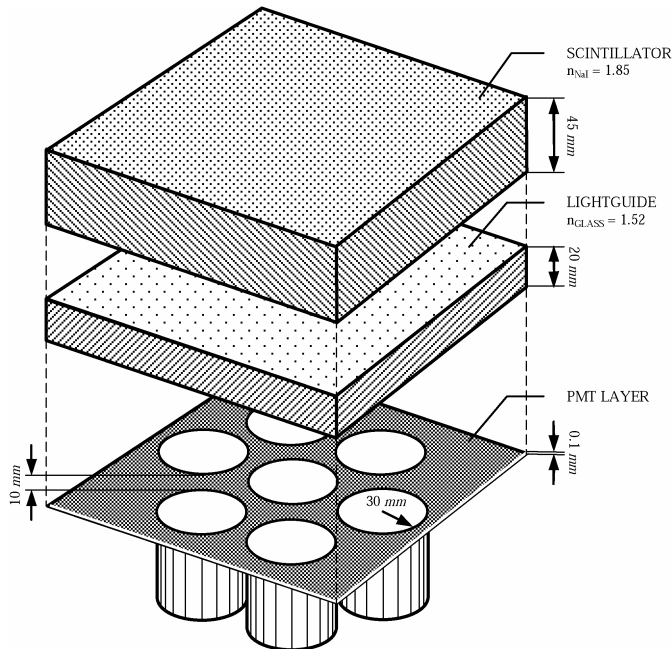


Fig. 3. Detached NaI scintillation detector used in the simulation.

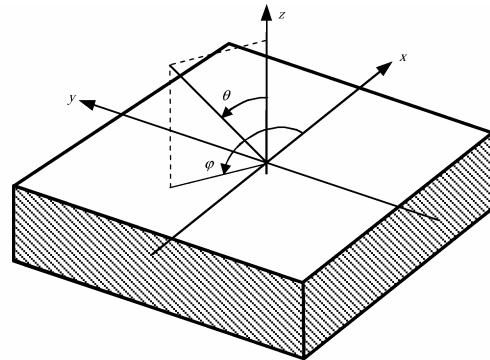


Fig. 5. Incidence angle measurement: normal angle θ and azimuthal angle ϕ .

Four tests were performed in order to analyze the effectiveness of different scintillation coordinates estimation algorithms. The tests were performed in small regions of the detector. In each test, two sets of data were simulated: a training set and a test set.

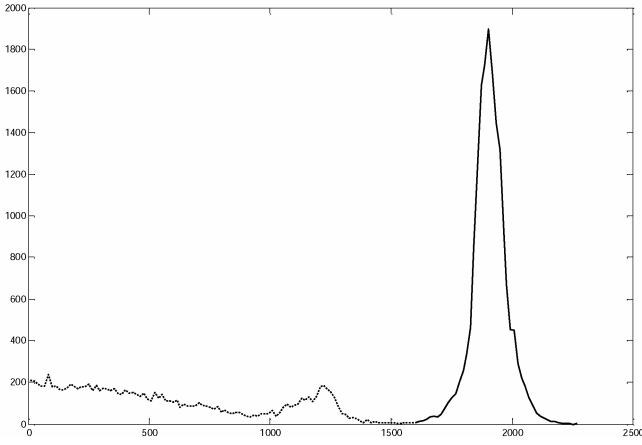


Fig. 6. Estimated pulse spectrum: number of scintillation events vs. the number of photoelectrons produced in an event. Events below the photopeak (dotted) were rejected.

The training set consisted of simulated PMT responses to scintillation events resulting from gamma quanta impinging at the crystal surface on an evenly-spaced grid (31×31 points with 1mm step, 500 gamma quanta per grid point). The test set was used for error estimation and error distribution analysis in the entire tested region and was created on an evenly-spaced 16×16 grid with 2mm step, 5,000 gamma quanta per grid point.

The following tests were performed:

1. Region: [0mm,30mm]×[0mm,30mm],
Incidence angle: $\theta = 0^\circ$, $\varphi = 180^\circ$
2. Region: [0mm,30mm]×[0mm,30mm]
Incidence angle: $\theta = 10^\circ$, $\varphi = 180^\circ$
3. Region: [0mm,30mm]×[0mm,30mm]
Incidence angle: $\theta = 30^\circ$, $\varphi = 180^\circ$
4. Region: [40mm,-15mm]×[70mm,15mm]
Incidence angle: $\theta = 0^\circ$, $\varphi = 180^\circ$

Test 1 served as a reference. Tests 2 and 3 were used to examine the sensitivity to parallax effect. Test 4 was used to examine the influence of edge effects. The following scintillation coordinates estimation algorithms were compared:

- *Anger algorithm* with threshold pulse pre-amplification, which is used in many modern scintillation detectors [3], [12], [13]. The output of the Anger algorithm was corrected by an ideal infinitely-dense bias correction map (unachievable in practice).
- *Localized linear regression (LLR)*. Position estimation was carried out according to the formula:

$$y = a_0 + \mathbf{a}^T \mathbf{x}$$

where y is the estimated position (X coordinate), \mathbf{x} is the vector of PMT responses and (a_0, \mathbf{a}) is the vector of regression coefficients found by minimizing the MSE over the training set in the tested region:

$$\mathbf{a} = \underset{\mathbf{a}}{\operatorname{argmin}} \left\{ \sum_{i=1}^N (a_0 + \mathbf{a}^T \mathbf{x}^i - y^i)^2 \right\}$$

where $\{\mathbf{x}^i, y^i\}_{i=1}^N$ is the training set.

- *Multilayer perceptron (MLP)* with 3 non-linear (tanh) layers (10 neurons each) and one linear neuron, implemented using the MathWorks MATLAB NN Toolbox [14].
- *Radial basis function network (RBF)* with 100 Gaussian neurons, implemented using the MATLAB RBF toolbox by Rättsch et al [10].

In all algorithms, the input was a vector of 7 PMT responses and the output was the X coordinate of the estimated LOF entrance position. Root mean squared (RMS) estimation error was calculated at each node of the test set grid according to

$$\text{RMS} = \left[\frac{1}{N} \sum_{i=1}^N (\hat{y}^i - y^i)^2 \right]^{1/2}$$

Minimum, maximum and average RMS error over the test set grid was found. Position estimation error histogram was computed on the data of the test set and error distribution parameters such as bias (mean error), RMS error, standard deviation and FWHM were estimated.

The Influence of multiple interactions

An additional test (Test 5) was performed to study the influence of multiple interactions in the scintillation crystal on scintillation position estimation accuracy. For this purpose, a test set, consisting of 100,000 gamma quanta impinging the crystal at incidence angle $\theta = 30^\circ$ in the center of the region used in Test 3, was generated. For each event, the total number of interactions, of which it comprised, was recorded. Then, the test set was divided into subsets containing events with fixed number of interactions (from 1 to 5). RMS error of the estimators obtained in Test 3 was calculated on these sets.

VI. RESULTS

Tables I-VI show the estimation error distribution parameters for different algorithms obtained in Tests 1-4, respectively. Figures 7-10 show the position estimation error histograms obtained in Tests 1-4, respectively. All the histograms are normalized by the peak value to make easier FWHM comparison.

Anger algorithm appeared the worst method in all tests. Local linear regression, which did not appear to be the best among the compared adaptive estimation algorithms, yielded in all tests better results than Anger's algorithm. This fact emphasizes the importance of locality. Non-linear estimation, using MLP and RBF networks, showed the best results in all tests.

The best non-linear methods showed about 33%, 40%, 54% and 11% of improvement in the RMS error compared to the Anger algorithm in Tests 1-4, respectively. The improvement rose with the incidence angle and was especially significant in Test 3 (incidence angle 30°). This fact demonstrates the ability of our method to treat large-incidence-angle events more accurately than the Anger algorithm.

Error distributions produced by the non-linear estimators

tend to have smaller FWHM:standard deviation ratio compared to that of the Anger algorithm; this can potentially result in additional image resolution improvement [11].

Figure 11 demonstrates the RMS error in Test 5 as function of the number of interactions in the crystal. ANN estimators appear to be less sensitive to multiple interactions than the Anger algorithm.

TABLE I
ERROR DISTRIBUTION – TEST 1 ($\theta=0^\circ$)

| | Bias (mm) | RMS Error (mm) | Std. Deviation (mm) | FWHM (mm) |
|-------|--------------|-------------------|---------------------------|--------------|
| Anger | — | 5.8185 | 5.8185 | 8.86 |
| LLR | 0.4927 | 4.1869 | 4.1579 | 4.49 |
| MLP | 0.0070 | 3.8833 | 3.8832 | 3.63 |
| RBF | 0.0563 | 4.0083 | 4.0080 | 4.40 |

TABLE II
ERROR DISTRIBUTION – TEST 2 ($\theta=10^\circ$)

| | Bias (mm) | RMS Error (mm) | Std. Deviation (mm) | FWHM (mm) |
|-------|--------------|-------------------|---------------------------|--------------|
| Anger | — | 6.5805 | 6.5805 | 11.26 |
| LLR | 0.8106 | 4.2798 | 4.2025 | 6.17 |
| MLP | 0.1601 | 4.1601 | 4.1572 | 5.18 |
| RBF | 0.6935 | 4.0225 | 3.9624 | 5.75 |

TABLE III
ERROR DISTRIBUTION – TEST 3 ($\theta=30^\circ$)

| | Bias (mm) | RMS Error (mm) | Std. Deviation (mm) | FWHM (mm) |
|-------|--------------|-------------------|---------------------------|--------------|
| Anger | — | 10.8209 | 10.8209 | 25.30 |
| LLR | -1.0584 | 5.3644 | 5.2590 | 10.75 |
| MLP | 0.2323 | 4.9454 | 4.9400 | 13.39 |
| RBF | 0.5754 | 5.0396 | 5.0067 | 8.23 |

TABLE IV
ERROR DISTRIBUTION – TEST 4 (PERIPHERAL REGION, $\theta=0^\circ$)

| | Bias (mm) | RMS Error (mm) | Std. Deviation (mm) | FWHM (mm) |
|-------|--------------|-------------------|---------------------------|--------------|
| Anger | — | 11.8644 | 11.8644 | 26.76 |
| LLR | -0.2680 | 5.2147 | 5.2078 | 8.71 |
| MLP | -0.0596 | 4.3069 | 4.3065 | 5.13 |
| RBF | -0.3079 | 4.2259 | 4.2147 | 6.69 |

VII. COMPUTATIONAL COMPLEXITY

MLP network used in this work performs 280 multiplications, 31 additions and 30 computations of the non-linear function per detected photon. Non-linear function can be efficiently computed using look-up tables and, in general, its computation is estimated as 5-6 multiplication operations. Preliminary coarse scintillation position estimation and network selection can be carried out in practically negligible time. Hence, about 500 FLOPs are required per scintillation event.

The RBF networks used in this work require about 700 additions, 100 multiplications and 100 computations of the non-linear function, which requires about 1000 FLOPs per

scintillation event.

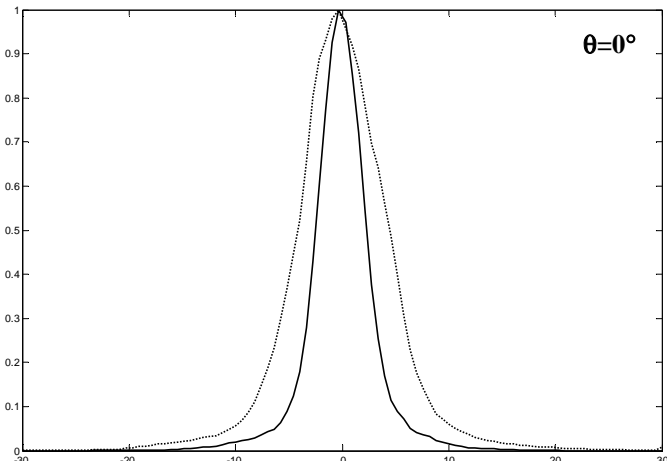


Fig. 7. Error histogram of the unbiased Anger algorithm (dashed) and the best ANN estimator (solid) in Test 1. X-axis represents error in mm.

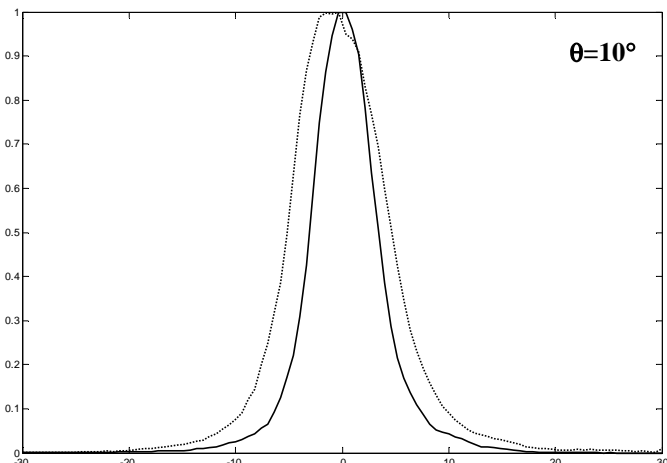


Fig. 8. Error histogram of the unbiased Anger algorithm (dashed) and the best ANN estimator (solid) in Test 2. X-axis represents error in mm.

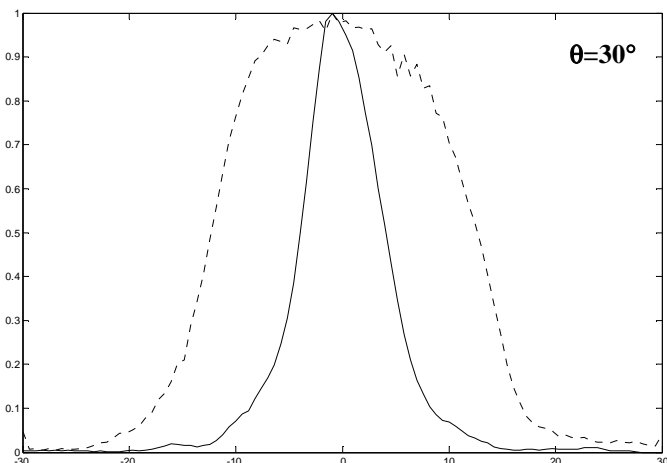


Fig. 9. Error histogram of the unbiased Anger algorithm (dashed) and the best ANN estimator (solid) in Test 3. X-axis represents RMS error in mm.

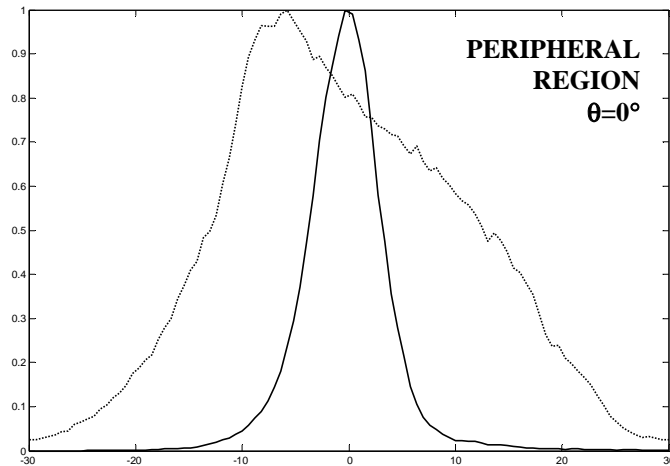


Fig. 10. Error histogram of the unbiased Anger algorithm (dashed) and the best ANN estimator (solid) in Test 4. X-axis represents RMS error in mm.

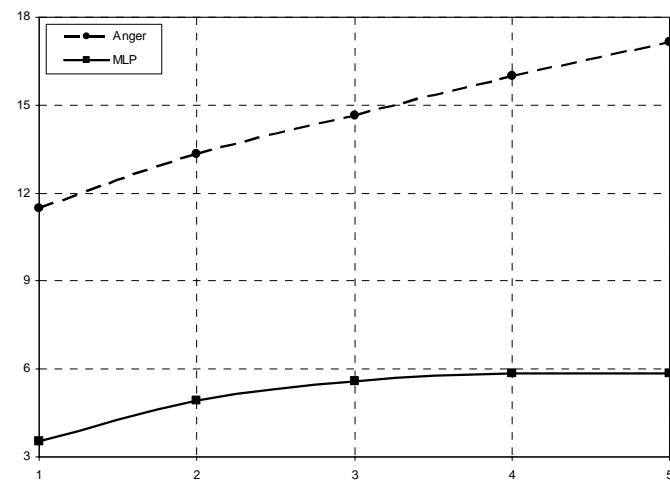


Fig. 11. Test 5: RMS error in mm vs number of interactions. Anger algorithm (dashed) and the best ANN estimator (solid).

A 1 GFLOPS processor would be capable of handling about 1×10^6 events per second, which is sufficient for PET applications. Since most artificial neural network types have a highly parallelizable pipeline-like architecture, implementation using dedicated hardware may be advantageous.

VIII. CONCLUSIONS

The proposed method of LOF estimation, based on artificial neural networks, incorporates information about the incidence angle in the estimation algorithm. Unlike the conventional algorithms, which estimate the scintillation coordinates, our approach estimates directly the photon line of flight, given PMT responses from a pair of detectors. This allows compensation for the parallax effect, multiple Compton scattering and increases effective detection area.

In practice, a different version of the algorithm can be implemented. The neural networks can be fed with the angle as additional input and trained over small regions of the detector on a range of angles with given angular resolution. The use of localized estimators allows reduce the complexity of each estimator. The proposed algorithm is sufficiently fast to be

implemented in real time using standard software or hardware.

APPENDIX

The following neural network architectures were used in this work:

1. Multi-layer perceptron (MLP), shown in Figure 12:

$$y_k^n = \sum_{i=1}^{N_{n-1}} \varphi(w_{k,n}^i y_i^{n-1}) + b_{k,n} \quad ; \quad y_k^0 = x_k$$

$$\Phi = \sum_{i=1}^{N_{L-1}} w_L^i y_i^{L-1} + b_L,$$

where L is the number of layers; N_l is the number of neurons in each layer; y_k^n and $x_{k,n}, b_{k,n}$ are the output and the parameter vector of k -th neuron in n -th layer, respectively; x and Φ are the network input and output, respectively; φ is some non-linear function, usually of a sigmoidal type [7].

2. Radial basis function (RBF) network, shown in Figure 13:

$$\Phi = \sum_{k=1}^N w_k \beta(d(x, c_k); \sigma_k) + b,$$

where N is the number of neurons in the non-linear layer; $\{w, b\}$ are the network weights; β is a Gaussian with controllable variance, σ_k , and mean, c_k [7].

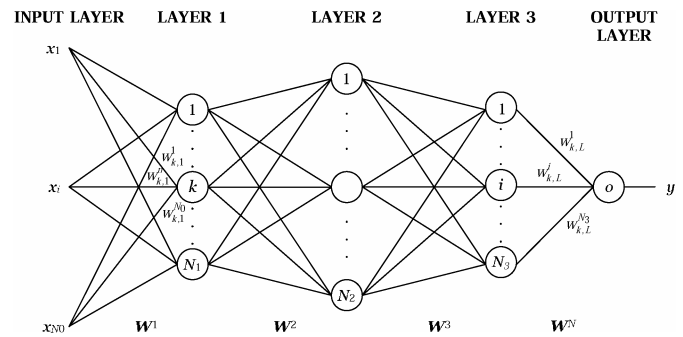


Fig. 12. Multilayer perceptron with three hidden layers and single output neuron.

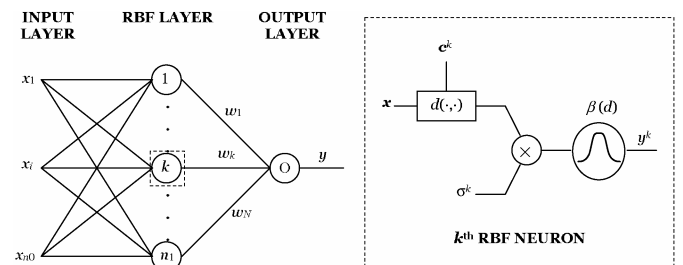


Fig. 13. RBF network with single output neuron.

REFERENCES

- [1] H. O. Anger, "Scintillation camera", Rev. Sci. Instr., vol. 29, pp. 27-33, 1958
- [2] W. R. Cook, M. Finger and T. A. Prince, "A thick Anger camera for gamma-ray astronomy", IEEE Trans. Nucl. Sci., vol. NS-32, pp. 129-133, 1985

- [3] H. Barrett and W. Swindell, *Radiological imaging*, Academic Press, 1981
- [4] T. Tomitani, Y. Futami, Y. Iseki, S. Kouda, T. Nishio, T. Murakami, A. Kitagawa, M. Kanazawa, E. Urakabe, M. Shinbo and T. Kanai, "Depth encoding of point-of-interaction in thick scintillation cameras", *Proc. of IEEE MIC*, Seattle, WA, 1999.
- [5] S. Delorme, R. Frei, C. Joseph, J.-F. Loude and C. Morel, "Use of a neural network to exploit light division in a triangular scintillating crystal", *Nuclear Instruments and Methods in Physics Research A* 373, pp. 111-118, 1996
- [6] D. Clément, R. Frei, J.-F. Loude and C. Morel, "Development of a 3D position sensitive scintillation detector using neural networks", *Proc. of the IEEE Med. Imag. Conf.*, Toronto, November 1998.
- [7] S. Haykin, *Neural networks: a comprehensive foundation*, 2nd ed., Prentice Hall, 1999
- [8] T. Levin and C. Moisan, "A crash course on using the TRIUMF detector modeling platform", Triumf, Canada's National Laboratory for Particle and Nuclear Physics, November 1996.
- [9] G. Tsang, C. Moisan and J. G. Rogers, "A simulation to model positron encoding multicrystal PET detectors", *IEEE Trans. Nucl. Sci.*, vol. 42, no. 6, pp. 2236-2242, December 1995.
- [10] K. R. Müller, A. Smola, G. Rätsch, B. Schölkopf, J. Kohlmorgen and V. Vapnik, "Using support vector machines for time series prediction", *Advances in kernel methods – support vector learning*, MIT Press, 1998.
- [11] A. M. Bronstein, M. M. Bronstein, M. Zibulevsky and Y. Y. Zeevi, "High energy photon detection in PET using neural networks", Research Report, Technion, 2002. Available: <http://visl.technion.ac.il/bron/works>
- [12] G. Kulberg and G. Muehlechner, "Scintillation camera with improved resolution", U.S. Patent 3732419, May 8, 1973.
- [13] D. Inbar, "Method and means for improving the resolution of a gamma camera", French Patent 2530824, Jan. 27, 1984.
- [14] The MathWorks Inc., "ANN toolbox user's guide", Sep. 2000.